



Heat transfer in Oldroyd-B fluid flow due to an exponentially stretching wall utilizing Cattaneo–Christov heat flux model

M. Mustafa¹ · T. Hayat^{2,3} · A. Alsaedi³

Received: 4 September 2017 / Accepted: 13 March 2018 / Published online: 20 March 2018
© The Brazilian Society of Mechanical Sciences and Engineering 2018

Abstract

Here we are concerned with the Oldroyd-B fluid flow resulting from the deformation of a non-isothermal flat surface with exponentially varying velocity. The objective is to resolve the heat transfer problem by assuming an exponentially varying wall temperature. A non-Fourier model is followed that enables one to investigate the features of thermal relaxation time phenomenon. Using local similarity method, the governing system is changed to a set of locally similar equations which have been tackled by optimal homotopy analysis method. The solution profiles are obtained and elucidated for broad parameter values. The direction and amount of heat flow are governed by a parameter measuring the exponential growth/decay rate of wall temperature with horizontal distance. An important implication of this research is that thermal field is substantially altered by thermal relaxation time. Also, the change in temperature profiles with variation in other parameters become prominent as thermal relaxation time enlarges. A comparative study of current computations with the existing literature appears convincing.

Keywords Heat transfer · Stretching boundary · Series solution · Polymeric liquid

1 Introduction

Non-Newtonian fluids are frequently encountered in daily life and in industrial processes, for instance, in chemical, food processing and oil industries. A particular characteristic of some non-Newtonian liquids is the retention of fading “memory” upon the removal of stress which is termed as fluid’s elasticity. Viscoelastic fluids contain normal stress effects which are an expression of fluid’s elasticity which is added to the viscous effect when the fluid is set in motion. There are strong experimental

manifestations to the viscoelastic behavior such as Weissenberg or rod-climbing effect. Commonly encountered examples are clay coatings, food products, inks, detergents, food gels, gums, emulsions, liquid polymers, liquid crystals, etc. One of the frequently employed viscoelastic models is the Oldroyd-B fluid model that can predict the behaviors of relaxation time, creep and normal stress differences for many polymeric liquids. In recent past, modest research is published concerning boundary layer analysis in Oldroyd-B liquid, compared with its Newtonian counterpart. Bhatnagar et al. [1] studied the boundary layer formation in Oldroyd-B fluid near a linearly stretched sheet with stream-wise pressure gradient. In this work, the authors used perturbation expansions for non-dimensional velocity and extra stress tensor components in terms of small viscoelastic fluid parameter. Further, graphical results addressing the behavior of fluid’s elasticity were obtained and deliberated. Later, Sajid et al. [2] evaluated explicit expressions of stress tensor components for Oldroyd-B model. These components were then used to formulate stagnation-point flow of Oldroyd-B fluid near stretching plate. Finally, they managed to find finite difference approximations of resulting boundary value problem. Shehzad et al. [3] considered thermophoretic particle

Technical Editor: Cezar Negro.

✉ M. Mustafa
meraj_mm@hotmail.com; merajmustafa@sns.nust.edu.pk

¹ School of Natural Sciences (SNS), National University of Sciences and Technology (NUST), Islamabad 44000, Pakistan

² Department of Mathematics, Quaid-I-Azam University 45320, Islamabad 44000, Pakistan

³ Department of Mathematics, Faculty of Science, King Abdulaziz University, P. O. Box 80257, Jeddah 21589, Saudi Arabia

deposition in three-dimensional Oldroyd-B fluid flow adjacent to a bi-directional deforming sheet. Series and numerical solutions for Oldroyd-B fluid motion over a stationary plate with stream-wise pressure gradient were computed by Abbasbandy et al. [4]. Effects of variable thermal conductivity on the Oldroyd-B fluid motion across an impulsively stretching surface were deliberated in Motsa and Ansari [5]. Recent attempts in the area can be stated through [6–13] and refs. there in.

Heat transfer refers to the transmission of thermal energy from one region to another as a result of temperature gradient. This phenomenon is associated with flows in wide spectrum of industrial and geophysical processes. Fourier law [14], developed in 1822, gives the relation between heat flow rate and the temperature gradient and it is recognized as fundamental law of conduction. This law gives a paradoxical prediction that any initial change would instantly alter the medium under observation and, therefore, it does not preserve the “causality principle”. This questions whether or not Fourier law gives adequate description of the heat transport phenomenon. To resolve this shortcoming, Cattaneo [15] came up with the concept of heat transmission due to thermal waves travelling at finite speed. He included a partial time derivative in Fourier model that rendered a damped hyperbolic energy equation. Such kind of heat transfer description has important implications in everyday life, in fields such as modeling skin burn [16], nanofluid flows [17] and biological materials [18]. To ensure objectivity principle, Christov [19] modified the partial time derivative in Cattaneo model with frame indifferent objective rate. Cattaneo–Christov theory still seems incomplete since it does not account for the thermal retardation time which is the time required for the build-up of temperature gradient in a volume element. Straughan [20] investigated the Christov’s relation for convection heat transfer in Newtonian fluid with gravity acting downward. Tibullo and Zampoli [21] proved uniqueness theorem for incompressible fluid flow in a bounded domain with a non-Fourier heat flux. Haddad [22] employed the Cattaneo–Christov heat flux theory to analyze thermal instability threshold for viscous flow through Brinkman porous space separated by two infinite plane surfaces. Han et al. [23] made use of analytic and numeric schemes to deal with slip flow of Maxwell fluid considering non-Fourier heat conduction. Khan et al. [24] numerically analyzed heat flux relaxation effect on Maxwell fluid flow near an exponentially deforming non-isothermal wall. Hayat et al. [25] employed non-Fourier approach to analyze fluid flow near a surface with variable thickness. An analytical investigation of Christov’s equation for unsteady MHD flow between coaxially rotating disk was made by Hayat et al. [26]. Their computations revealed that radial stretching rate has a considerable

influence on velocity and temperature between the disks. Subsequent works in this area can be found in [27–35].

Heat transfer in boundary layer adjacent to continuously stretching surfaces with a given temperature has been a widely addressed research topic in fluid mechanics. It is important in a number of manufacturing processes such as glass-fiber and paper production, annealing of copper wire, condensation process, die forging and few others. Following the pioneering work of Crane [36], abundant material concerning interesting features of this problem is published. Magyari and Keller [37] described fluid flow over a non-isothermal surface which stretches in its own plane with exponentially varying velocity. Their results depict that structure of temperature curves is controlled by a parameter (A) measuring the exponential growth/decay of the wall temperature. After careful analysis, they concluded that meaningful solutions are possible only when this parameter is greater than a certain critical value. At this critical value of A , wall temperature gradient becomes zero illustrating that no heat transfer takes place between fluid and the surface. Later, Elbashbeshy [38] revisited the similarity analysis of Ref. [37] by assuming permeable stretching surface. Viscoelastic fluid flow caused by an exponentially stretching isothermal wall was analytically explored by Khan and Sanjayanand [39]. Radiation effects in viscous flow characterized by exponentially deforming boundary were elucidated by Sajid and Hayat [40] using homotopy approach. Bhattacharyya [41] found multiple solutions for steady flow driven by an exponentially shrinking wall. Recently, several fascinating heat transfer problems involving exponentially deforming surfaces have been published (see, for instance, Liu et al. [42], Mustafa et al. [43], Weidman [44], Ahmad et al. [45], Patil et al. [46], Merkin et al. [47], etc.).

To the best of authors’ knowledge, the Oldroyd-B fluid flow due to exponentially deforming surface has not been explored in the existence of thermal relaxation effects. Thus framework of Ref. [9] has been extended by involving Cattaneo–Christov heat flux theory. We rely on homotopy analysis approach, proposed by Liao [48, 49], to find analytical approximations for velocity and temperature profiles. Additionally, we use the concept of squared residuals to compute optimal results for convergence control parameters. Furthermore, we will seek the critical range of temperature exponent parameter for which the meaningful solution cannot be found. The main interest is to elucidate flow and thermal fields in the existence of key physical attribute of the problem namely thermal relaxation time. The computational results of wall shear stress and heat transfer rate are presented and elucidated for certain values of embedded quantities. The results of this study might be beneficial in polymer processing and coating-related applications.

2 Mathematical model

Consider a two-dimensional Oldroyd-B fluid flow over an impermeable plane wall at $y = 0$ expanding with velocity $u_w = u_0 e^{x/L}$. The incompressible Oldroyd-B fluid is contained in the region $y > 0$. The resulting motion of the quiescent fluid is produced solely by the stretching wall (see Fig. 1). Let the temperature at the wall vary with horizontal distance x according to $T_w = T_\infty + T_0 e^{Ax/2L}$, in which A is a constant whose value depends on the material properties of the fluid and T_∞ is the quiescent fluid temperature. A non-Fourier heat flux model due to Christov [19] is opted to analyze the thermal field. In view of these assumptions, the governing equations of Oldroyd-B motion and energy balance can be put in the following forms:

$$u_x + v_y = 0, \tag{1}$$

$$uu_x + vu_y + \lambda_1(u^2 u_{xx} + v^2 u_{yy} + 2uvu_{xy}) = v[u_{yy} + \lambda_2(uu_{xyy} + vu_{yyy} - u_x u_{yy} + u_y u_{xy})], \tag{2}$$

$$\rho C_p (v_i T_{,i}) = -Q_{i,i}, \tag{3}$$

where v represents the kinematic viscosity of the fluid, ρ is the fluid density, λ_1 stands for fluid relaxation time, λ_2 for fluid retardation time, β_T is the volumetric expansion coefficient, C_p represents the specific heat capacity and Q_i denotes the heat flux vector. Christov [19] proposed the following heat conduction model:

$$\tau(Q_{i,t} + v_j Q_{i,j} - Q_j v_{i,j} + Q_i v_{j,j}) = -Q_i - \kappa T_i, \tag{4}$$

in which τ denotes the thermal relaxation time defined as the time lag required for the onset of heat conduction in a fluid element after temperature difference is assigned through it. Taking divergence of Eq. (4) and then utilizing Eq. (3), a simple arrangement yields the following result (see Han et al. [23], Khan et al. [24], etc.):

$$(uT_x + vT_y) + \tau \left(\begin{aligned} &u^2 T_{xx} + v^2 T_{yy} + 2uvT_{xy} + \\ &uu_x T_x + vu_y T_x + uv_x T_y + vv_y T_y \end{aligned} \right) = \alpha T_{yy}, \tag{5}$$

where α is the thermal diffusivity. Boundary conditions for problem under consideration are expressed below:

$$u(x, 0) = u_w(x) = U_0 \exp\left(\frac{x}{L}\right), v(x, 0) = 0, \tag{6a}$$

$$T(x, 0) = T_w(x) = T_\infty + T_0 \exp\left(\frac{Ax}{2L}\right), \tag{6b}$$

$$u(x, +\infty) = 0, T(x, +\infty) \rightarrow T_\infty, \tag{6c}$$

where conditions prescribed in Eq. (6a) indicate no slip and no penetration at the surface, Eq. (6b) signifies no thermal slip at the surface and Eq. (6c) shows that velocity and temperature gradients become zero far from the surface.

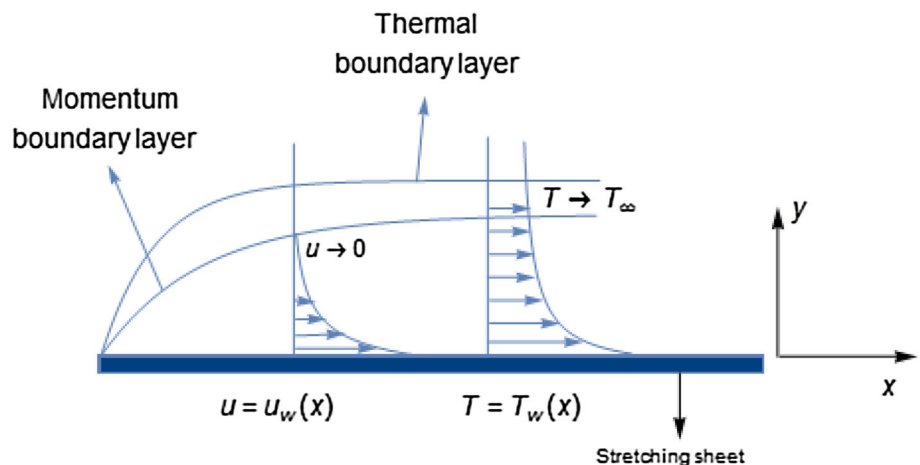
Let us introduce a transformation comprising non-dimensional quantities ψ, θ and ζ such that:

$$\begin{aligned} \zeta &= \sqrt{\frac{U_0}{2\nu L}} \exp\left(\frac{x}{2L}\right) y, \psi(x, y) \\ &= (2\nu L U_0)^{1/2} f(\zeta) \exp\left(\frac{x}{2L}\right), \theta(\zeta) = \frac{T - T_\infty}{T_w - T_\infty}. \end{aligned} \tag{7}$$

The axial and transverse velocity components are thus related to ψ according $u = \psi_y$ and $v = -\psi_x$ respectively. Substitution of above variables in Eqs. (2) and (5) gives rise to the following differential equations:

$$\begin{aligned} f''' - 2f'^2 + ff'' - \frac{\beta_1}{2}(4f'^3 - \zeta f'^2 f'' + f^2 f''' - 6ff' f'') \\ + \frac{\beta_2}{2}(3f''^2 + 2f' f''' - ff^{iv}) \\ = 0, \end{aligned} \tag{8}$$

Fig. 1 Physical configuration and coordinate system



$$\frac{1}{Pr} \theta'' + f \theta' - A f' \theta + \frac{\gamma}{2} [A f f'' \theta - A(A + 2) f'^2 \theta + (1 + 2A) f f' \theta' - f^2 \theta''] = 0. \tag{9}$$

Here β_1 denotes the non-dimensional fluid relaxation time which measures the ratio of time scale of material’s response to the observation time scale, β_2 represents the dimensionless retardation time which measures the time required for the build-up of shear stress in the fluid, γ is the non-dimensional thermal relaxation time and Pr stands for Prandtl number which is ratio of momentum diffusion to the thermal diffusion. These parameters are defined as follows:

$$Pr = \frac{\nu}{\alpha}, \quad \beta_1 = \frac{\lambda_1 u_w}{L}, \quad \beta_2 = \frac{\lambda_2 u_w}{L}, \quad \gamma = \frac{\tau u_w}{L}. \tag{10}$$

The transformed conditions are given below:

$$f = 0, \quad f' = 1, \quad \theta = 1 \quad \text{at} \quad \zeta = 0, \\ f' \rightarrow 0, \quad \theta \rightarrow 0 \quad \text{as} \quad \zeta \rightarrow \infty. \tag{11}$$

3 Series solutions by HAM

In this section, we look for series solutions of coupled non-linear equations $\mathcal{N}_f(f(\eta)) = 0$ (Eq. 8) and $\mathcal{N}_\theta(\theta(\eta)) = 0$ (Eq. 9) subject to the conditions (11) through homotopy analysis technique. On the basis of so-called “rule of solution expression” and the conditions (11), it is reasonable to set following initial approximations f_0 and θ_0 of functions f and θ , respectively:

$$f_0(\zeta) = 1 - \exp(-\zeta), \theta_0(\zeta) = \exp(-\zeta). \tag{12}$$

Let us choose the auxiliary linear operators \mathcal{L}_f and \mathcal{L}_θ of the following forms:

$$\mathcal{L}_f \equiv \frac{\partial^3}{\partial \zeta^3} - \frac{\partial}{\partial \zeta}, \quad \mathcal{L}_\theta \equiv \frac{\partial^2}{\partial \zeta^2} - 1. \tag{13}$$

The procedure outlined in Ref. [10] is exactly followed to reduce non-linear Eqs. (8) and (9) to n linear sub-problems containing an auxiliary parameter \hbar . These are solved exactly by MATHEMATICA for $n = 1, 2, 3, \dots$ and then homotopy series for f and θ are constructed as follows:

$$f(\zeta) = f_0(\zeta) + \sum_{n=1}^{\infty} f_n(\zeta), \tag{14}$$

$$\theta(\zeta) = \theta_0(\zeta) + \sum_{n=1}^{\infty} \theta_n(\zeta), \tag{15}$$

where $f_n(\zeta)$ and $\theta_n(\zeta)$ denote the solutions for n th-order deformation equations of Eqs. (8) and (9), respectively. It is well-known that convergence of homotopy series relies on the appropriate selection of parameter \hbar (see Liao [49]). In some articles [50–54], the method of finding optimal value of auxiliary parameter \hbar was introduced. Following these, we define the squared residuals of Eqs. (8) and (9) as follows:

$$\Delta_N^f(\hbar) = \int_0^\infty \left[\mathcal{N}_f \left(\sum_{j=0}^N f_j(\zeta) \right) \right] d\zeta, \tag{16}$$

$$\Delta_N^\theta(\hbar) = \int_0^\infty \left[\mathcal{N}_\theta \left(\sum_{j=0}^N \theta_j(\zeta) \right) \right] d\zeta. \tag{17}$$

Now we seek the values of \hbar for which squared residuals Δ_N^f and Δ_N^θ are minimum. This can be done through the command *Minimize* of the software MATHEMATICA as explained in Liao [50]. In Tables 1 and 2, we enlist the optimal values of \hbar for functions f and θ at different parameter values. It can be seen that reasonably accurate approximation to the exact solution is found for both low and high values of embedded parameters.

4 Results and discussion

A non-Fourier heat flux theory is utilized to model the flow and heat transfer of Oldroyd-B fluid bounded by an exponentially deforming non-isothermal surface. The arising local similarity equations have been dealt by well-known homotopy analysis technique. The accuracy of analytical scheme is validated by comparing the values of $f''(0)$ and $\theta'(0)$ to those reported by Khan et al. [24] via numerical approach. Table 3 demonstrates excellent correlation between analytical and numerical results which establishes the correctness of our code. We now turn our attention to examine the role of physical parameters on the flow and thermal fields. In Table 4, we provide numerical results for temperature gradient at the wall for various parameter values. In accordance with the study [37], the similarity solutions remain physically realistic for positive values of A , that is, heat flows from the stretching boundary towards the ambient fluid when $A > 0$. Wall temperature gradient has a positive value when parameter A is less than certain value A_c illustrating that temperature distribution is strictly convex and forms a “hill-shaped” pattern near the boundary which is referred as “Sparrow–Gregg hill”. Table 2 indicates that magnitude of $\theta'(0)$ grows with

Table 1 Optimal values of h for function f and corresponding squared residuals for different values of β_1 and β_2 at 13th-order of approximations when $A = \gamma = 0.5$ and $Pr = 1$

β_1	β_2	Optimal h for $f(\eta)$	Δ_N^f	Optimal h for $\theta(\eta)$	Δ_N^θ
0	0.5	- 0.728	4.12×10^{-13}	- 0.932	8.60×10^{-9}
0.2		- 0.610	4.70×10^{-11}	- 0.724	2.77×10^{-9}
0.5		- 0.573	1.15×10^{-10}	- 0.683	1.38×10^{-9}
0.8		- 0.484	7.98×10^{-10}	- 0.546	4.42×10^{-9}
1.2		- 0.400	3.99×10^{-9}	- 0.458	1.06×10^{-6}
0.25	0	- 0.721	6.34×10^{-11}	- 0.772	1.62×10^{-10}
	0.2	- 0.701	1.88×10^{-11}	- 0.750	2.66×10^{-9}
	0.5	- 0.679	8.25×10^{-12}	- 0.780	6.22×10^{-9}
	0.8	- 0.578	1.65×10^{-11}	- 0.792	4.97×10^{-8}
	1.2	- 0.457	1.41×10^{-10}	- 0.695	5.96×10^{-7}

Table 2 Optimal values of h for functions f and θ and corresponding squared residuals for different values of A, Pr and γ at 13th-order of approximations when $\beta_1 = \beta_2 = 0.5$

A	Pr	γ	Optimal h for $\theta(\eta)$	Δ_m^θ
- 2	1	0.5	- 0.795	1.10×10^{-5}
- 1			- 0.766	4.85×10^{-7}
0			- 0.706	3.49×10^{-9}
1			- 0.649	6.14×10^{-10}
2			- 0.605	2.06×10^{-9}
0.5	0.4		- 0.642	5.10×10^{-6}
	0.7		- 0.662	2.54×10^{-7}
	1.5		- 0.708	1.56×10^{-6}
	2		- 0.745	2.0×10^{-5}
	3		- 0.806	2.4×10^{-4}
	0.5	0	- 0.664	4.74×10^{-8}
		0.2	- 0.642	1.68×10^{-9}
		0.8	- 0.675	2.64×10^{-8}
		1.0	- 0.663	1.05×10^{-7}
		1.2	- 0.655	3.68×10^{-7}

increasing thermal relaxation time. Moreover, the effect of fluid relaxation time is to enhance the wall temperature gradient.

Figure 2 shows the evolution of similarity profile f' for various values of Deborah number β_1 . For comparison purpose, the figure also includes the results for Newtonian fluid case. All the curves begin from their wall value 1 and asymptotically decay to zero outside the boundary layer. It is revealed that velocity at any location above the sheet decreases for increasing values of β_1 . It means that, by an increase in β_1 , velocity gradient at the surface is increased. Also, a considerable reduction in boundary layer thickness is depicted when β_1 enlarges. Physically, large values of β_1 implies that stress relaxation is slow in comparison with the

Table 3 Comparison of present computations of $\theta'(0)$ with those of Khan et al. [24] when $A = 1.5$ and $\beta_2 = 0$

Pr	β_1	γ	$\theta'(0)$	
			Numerical [24]	HAM
1	0	0.5	- 1.55096	- 1.55097
			- 1.46365	- 1.46365
	0.5	0	- 1.39552	- 1.39538
			- 1.06969	- 1.06954
0.7	0	0.5	- 1.46365	- 1.46365
		1	- 1.82605	- 1.82605
		0.5	- 1.22415	- 1.22405
	0.5	0	- 1.14357	- 1.14342
			- 1.08247	- 1.08224
			- 0.84128	- 0.84012
		0.5	- 1.14357	- 1.14342
		1	- 1.42710	- 1.42701

observation time scale. Thus boundary layer thickness does not develop as fast as for small Deborah number.

Figure 3 presents velocity curve as a function of similarity variable ζ for varying values of Deborah number β_2 . As Deborah number β_2 grows, u -velocity component is seen to increase at any location above the surface. This also means that momentum penetration depth is increased as the fluid retardation time grows.

Figure 4 plots temperature curves, represented by $\theta(\zeta)$, by changing the Deborah numbers β_1 and β_2 . Our numerical results indicate that transverse velocity component v decreases with increasing β_1 above the sheet. It means that less fluid is extracted from the region of lower temperature far from the boundary when β_1 is increased. This in turn reduces the heat transfer rate or the wall temperature gradient. The smaller gradient $\theta'(0)$ yields thicker thermal boundary layer as found in the Fig. 4. We also found a

Table 4 Computational results of $f''(0)$ and $\theta'(0)$ for various parameter values at $Pr = 1$

β_1	β_2	γ	A	$\theta'(0)$
0	0.25	0.25	1.5	- 1.39855
0.2				- 1.36866
0.4				- 1.34187
0.6				- 1.31751
0.25	0.1		0.5	- 0.84531
	0.2			- 0.86236
	0.4			- 0.89124
	0.6			- 0.91478
	0.25	0		- 0.77507
		0.2		- 0.85515
		0.4		- 0.92727
		0.6		- 1.00324
		0.25	0	- 0.59503
			0.7	- 0.97376
			1	- 1.23636
			1.5	- 1.36171

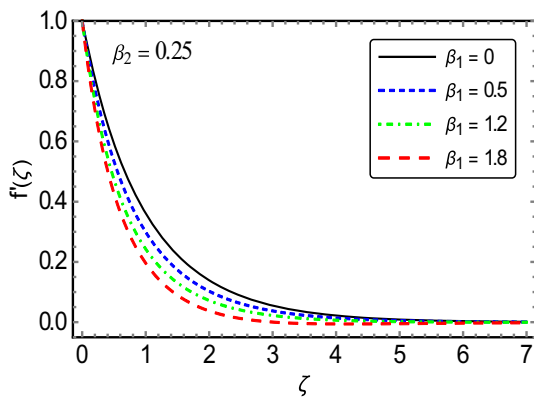


Fig. 2 Profiles of velocity field $f'(\zeta)$ for different values of β_1

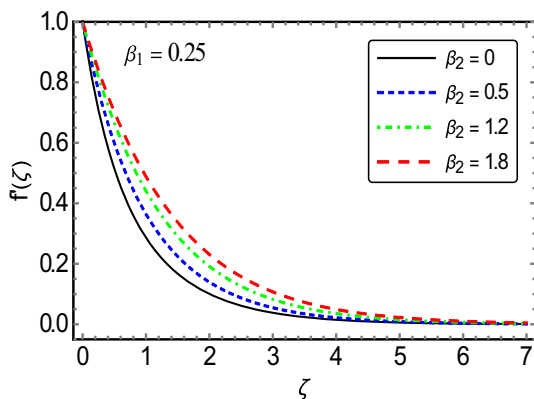


Fig. 3 Profiles of velocity field $f'(\zeta)$ for different values of β_2

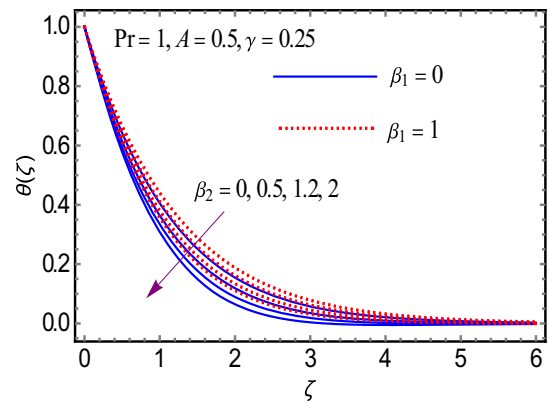


Fig. 4 Profiles of temperature field $\theta(\zeta)$ for various values of β_2

slight reduction in temperature profile θ for increasing values of retardation time λ_2 .

Figure 5 is plotted to inspect the change in temperature distribution $\theta(\zeta)$ as the dimensionless thermal relaxation time γ is varied. A considerable reduction in temperature profile is found for growing thermal relaxation time.

In Fig. 6, temperature curves are computed for different values of temperature exponent parameter A . When $A = -2$, heat flows from the quiescent fluid towards the stretching wall, a phenomenon that is signaled in the plot of θ by the existence of Sparrow–Gregg hills. We observe that temperature profile at $\zeta = 0$ is strictly convex when parameter A is strictly less than some negative value A_c while it is strictly concave for $A > 0$, as also noted in [37]. When $A = A_c$, the temperature curve represents the adiabatic situation. As expected, heat penetration in the fluid considerably decreases for increasing values of A .

Figures 7 and 8 portray the impact of Prandtl number Pr on the near-surface temperature for $A = 0.5$ and $A = -1.5$, respectively. Temperature profile $\theta(\zeta)$ becomes thinner when Pr enlarges. This is not surprising since increasing Prandtl number implies slower diffusion rate which in turn reduces heat penetration into the quiescent fluid. In Fig. 8,

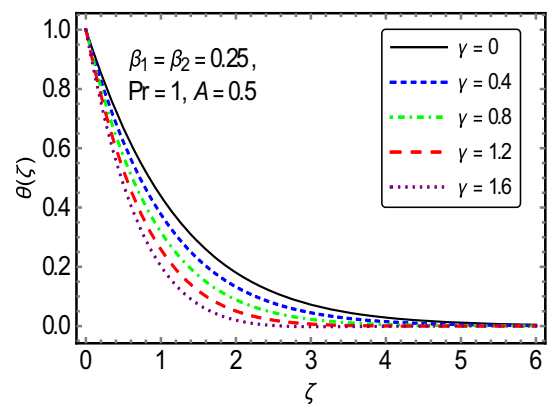


Fig. 5 Profiles of temperature field $\theta(\zeta)$ for various values of γ

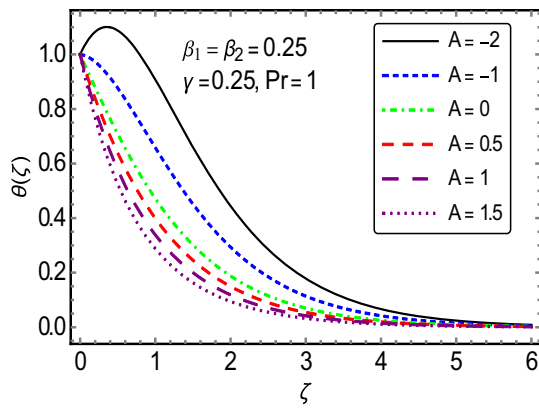


Fig. 6 Profiles of temperature field $\theta(\zeta)$ for different values of A

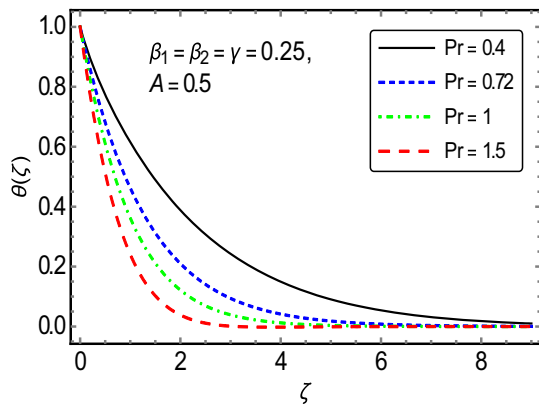


Fig. 7 Profiles of temperature field $\theta(\zeta)$ for different values of Pr when $A = 0.5$

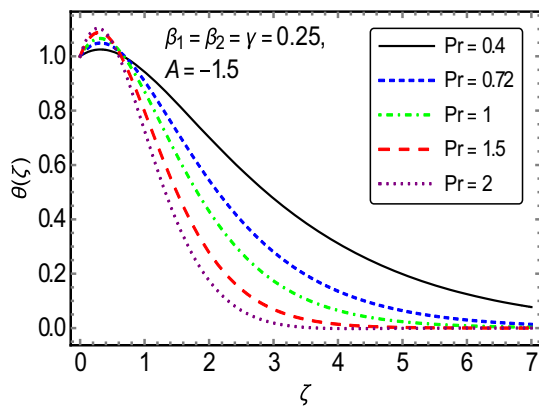


Fig. 8 Curves of wall temperature gradient $\theta'(0)$ for different values of Pr when $A = -1.5$

Sparrow–Gregg hills are evident just in the wall region and height of these hills increase with increasing Pr . Similar trend is also noticed in [37] for the Newtonian fluid case.

Figure 9 demonstrates the variation in wall temperature gradient $\theta'(0)$ with the change in Prandtl number Pr for different values of A . The black curve is computed at $A = A_c = -0.85$ for which $\theta'(0) = 0$. This illustrates that the

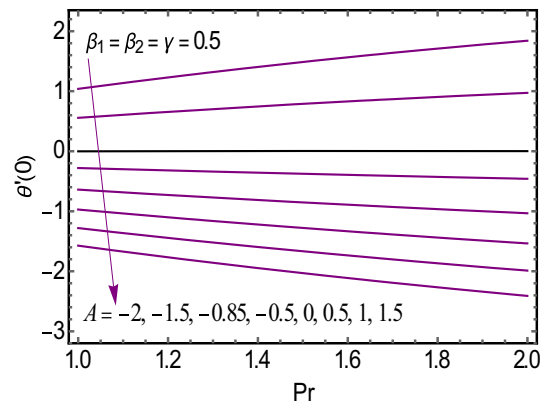


Fig. 9 Curves of wall temperature gradient $\theta'(0)$ for different values of A

stretching surface becomes adiabatic when $A = -0.85$. When $A < A_c = 0.85$, wall temperature gradient $\theta'(0)$ becomes positive for any value of Pr which is an indicator of the reverse heat flow near the wall region. Irrespective of the choice of A , the profile of $|\theta'(0)|$ continues to grow as Pr increases.

Figure 10 displays the graphs of $\theta'(0)$ versus dimensionless thermal relaxation time γ for varying Deborah number β_1 . The solid and dashed curves correspond to $\beta_2 = 0$ and $\beta_2 = 1$, respectively. Interestingly, a linear growth in the magnitude of $\theta'(0)$ with increasing β_1 is apparent. It should be noted here that variation in $\theta'(0)$ with β_1 increases in magnitude with increasing thermal relaxation time.

5 Concluding remarks

An analytical study is performed for flow of an incompressible Oldroyd-B fluid bounded by an exponentially deforming sheet. Oldroyd-B fluid model is considered to be

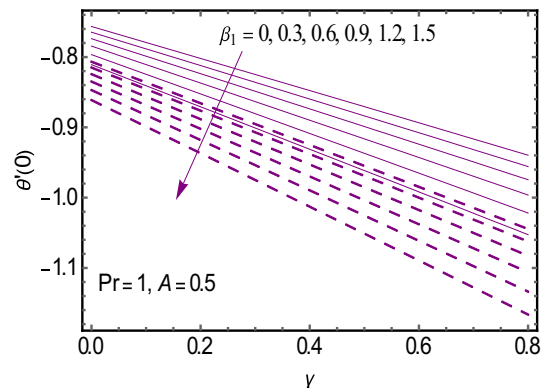


Fig. 10 Curves of wall temperature gradient $\theta'(0)$ for various values of γ

adequate in flow description of many polymeric liquids. Thus current analysis has obvious role in polymer extrusion and metal working processes. The temperature at the surface is assumed to grow or decay exponentially with the horizontal distance x . The main motivation was to inspect thermal field when the Cattaneo–Christov heat flux theory is involved. Important observations of this work are listed below:

- Both u -velocity component and boundary layer thickness decrease/increase when stress relaxation/retardation time is enhanced.
- The curvature of temperature field θ near the surface is strictly convex when temperature exponent parameter A is chosen beyond a certain value A_c that depends on the choice of other parameters. In this case, “Sparrow–Gregg hills” appear in the curves of $\theta(\zeta)$.
- When $A = A_c$, the stretching surface is “adiabatic” for any considered Prandtl number Pr .
- Irrespective of the choice of parameter A , heat penetration depth reduces and wall temperature gradient grows as Pr enlarges.
- A considerable decrease in temperature distribution is found when thermal relaxation time is increased.
- For increasing fluid relaxation time, thermal boundary layer becomes thinner and wall temperature gradient enlarges.
- The influences of parameters appear similar in both Cattaneo–Christov and Fourier models. However, the effects are prominent in Cattaneo–Christov model when compared with Fourier model.
- Present analytical findings appear to be consistent with the results of available articles in limiting cases.
- Following studies [55] and [56], current problem can be investigated for a nanoparticle working fluid in future. Further, this work can be revisited to focus on optimal results for drag coefficient and heat transfer rates (see [57] and [58] for details).

References

1. Bhatnagar RK, Gupta G, Rajagopal KR (1995) Flow of an Oldroyd-B fluid due to a stretching sheet in the presence of a free stream velocity. *Int J Non-Linear Mech* 30:391–405
2. Sajid M, Abbas Z, Javed T, Ali N (2010) Boundary layer flow of an Oldroyd-B fluid in the region of a stagnation point over a stretching sheet. *Can J Phys* 88:635–640
3. Shehzad SA, Alsaedi A, Hayat T, Alhuthali MS (2014) Thermophoresis particle deposition in mixed convection three-dimensional radiative flow of an Oldroyd-B fluid. *J Taiwan Inst Chem Eng* 45:787–794
4. Abbasbandy S, Hayat T, Alsaedi A, Rashidi MM (2014) Numerical and analytical solutions for Falkner–Skan flow of MHD Oldroyd-B fluid. *Int J Numer Methods Heat Fluid Flow* 24:390–401
5. Motsa SS, Ansari MS (2015) Unsteady boundary layer flow and heat transfer of Oldroyd-B nanofluid towards a stretching sheet with variable thermal conductivity. *Therm Sci* 19:239–248
6. Awad FG, Ahamed SMS, Sibanda P, Khumalo M (2015) The effect of thermophoresis on unsteady Oldroyd-B nanofluid flow over stretching surface. *PLoS One* 10:e0135914. <https://doi.org/10.1371/journal.pone.0135914>
7. Sandeep N, Kumar BR, Kumar MSJ (2015) A comparative study of convective heat and mass transfer in non-Newtonian nanofluid flow past a permeable stretching sheet. *J Mol Liq* 212:585–591
8. Zhang Y, Zhang M, Bai Y (2016) Flow and heat transfer of an Oldroyd-B nanofluid thin film over an unsteady stretching sheet. *J Mol Liq* 220:665–670
9. Hayat T, Imtiaz M, Alsaedi A (2016) Boundary layer flow of Oldroyd-B fluid by exponentially stretching sheet. *Appl Math Mech* 37:573–582
10. Abbasi FM, Mustafa M, Shehzad SA, Alhuthali MS, Hayat T (2016) Analytical study of Cattaneo-Christov heat flux model for a boundary layer flow of Oldroyd-B fluid. *Chin Phys B* 25:6. <https://doi.org/10.1088/1674-1056/25/1/014701>
11. Ahmad M, Ahmad I, Sajid M, Abbasi A (2016) Flow of an Oldroyd-B fluid past an unsteady bidirectional stretching sheet with constant temperature and constant heat flux. *J Appl Fluid Mech* 9:1329–1337
12. Sandeep N, Reddy MG (2017) MHD Oldroyd-B fluid flow across a melting surface with cross diffusion and double stratification. *Eur Phys J Plus* 132:147. <https://doi.org/10.1140/epjp/i2017-11417-9>
13. Hashmi MS, Khan N, Mahmood T, Shehzad SA (2017) Slip effects on MHD flow of a generalized Oldroyd-B fluid with fractional derivative. *Int J Therm Sci* 111:463–474
14. Fourier J (1822) *Theorie Analytique Da La Chaleur*, Paris
15. Cattaneo C (1948) Sulla conduzionedelcalore. *AttiSemin. Mat Fis Univ Modena Reggio Emilia* 3:83–101
16. Dai W, Wang H, Jordan PM, Mickens RE, Bejan A (2008) A mathematical model for skin burn injury induced by radiation heating. *Int J Heat Mass Transf* 51:5497–5510
17. Liu H, Bussmann M, Mostaghimi J (2009) A comparison of hyperbolic and parabolic models of phase change of a pure metal. *Int J Heat Mass Transf* 52:1177–1184
18. Saidane A, Aliouat S, Benzohra M, Ketata M (2005) A transmission line matrix (TLM) study of hyperbolic heat conduction in biological materials. *J Food Eng* 68:491–496
19. Christov CI (2009) On frame indifferent formulation of the Maxwell–Cattaneo model of finite speed heat conduction. *Mech Res Commun* 36:481–486
20. Straughan B (2010) Thermal convection with the Cattaneo–Christov model. *Int J Heat Mass Transf* 53:95–98
21. Tibullo V, Zampoli V (2011) A uniqueness result for the Cattaneo–Christov heat conduction model applied to incompressible fluids. *Mech Res Commun* 38:77–79
22. Haddad SAM (2014) Thermal instability in Brinkman porous media with Cattaneo–Christov heat flux. *Int J Heat Mass Transf* 68:659–668
23. Han S, Zheng L, Li C, Zhang X (2014) Coupled flow and heat transfer in viscoelastic fluid with Cattaneo–Christov heat flux model. *Appl Math Lett* 38:87–93
24. Khan JA, Mustafa M, Hayat T, Alsaedi A (2015) Numerical study of Cattaneo–Christov heat flux model for viscoelastic flow due to an exponentially stretching surface. *PLoS One* 10. <https://doi.org/10.1371/journal.pone.0137363>
25. Hayat T, Khan MI, Farooq M, Alsaedi A, Waqas M, Yasmeen T (2016) Impact of Cattaneo–Christov heat flux model in flow of

- variable thermal conductivity fluid over a variable thicked surface. *Int J Heat Mass Transf* 99:702–710
26. Hayat T, Qayyum S, Imtiaz M, Alsaedi A (2016) MHD flow and heat transfer between coaxial rotating stretchable disks in a thermally stratified medium. *PLoS One* 11. <https://doi.org/10.1371/journal.pone.0155899>
 27. Hayat T, Qayyum S, Imtiaz M, Alsaedi A (2017) Flow between two stretchable rotating disks with Cattaneo–Christov heat flux model. *Res Phys* 7:126–133
 28. Hayat T, Qayyum S, Imtiaz M, Alsaedi A (2016) Three-dimensional rotating flow of Jeffrey fluid for Cattaneo–Christov heat flux model. *AIP Adv* 6:025012. <https://doi.org/10.1063/1.4942091>
 29. Mushtaq A, Abbasbandy S, Mustafa M, Hayat T, Alsaedi A (2016) Numerical solution for Sakiadis flow of upper-convected Maxwell fluid using Cattaneo–Christov heat flux model. *AIP Adv* 6:015208. <https://doi.org/10.1063/1.4940133>
 30. Malik R, Khan M, Mushtaq M (2016) Cattaneo–Christov heat flux model for Sisko fluid flow past a permeable non-linearly stretching cylinder. *J Mol Liq* 222:430–434
 31. Rubab K, Mustafa M (2016) Cattaneo–Christov heat flux model for MHD three dimensional flow of Maxwell fluid over a stretching sheet. *PLoS One* 11. <https://doi.org/10.1371/journal.pone.0153481>
 32. Li J, Zheng L, Liu L (2016) MHD viscoelastic flow and heat transfer over a vertical stretching sheet with Cattaneo–Christov heat flux effects. *J Mol Liq* 221:19–25
 33. Abbasi FM, Shehzad SA (2016) Heat transfer analysis for three-dimensional flow of Maxwell fluid with temperature dependent thermal conductivity: application of Cattaneo–Christov heat flux model. *J Mol Liq* 220:848–854
 34. Liu L, Zheng L, Liu F, Zhang X (2017) Heat conduction with fractional Cattaneo–Christov upper-convective derivative flux model. *Int J Therm Sci* 112:421–426
 35. Mustafa M, Hayat T, Alsaedi A (2017) Rotating flow of Maxwell fluid with variable thermal conductivity: an application to non-Fourier heat flux theory. *Int J Heat Mass Transf* 106:142–148
 36. Crane LJ (1970) Flow past a stretching plate. *J Appl Math Phys (ZAMP)* 21:645–647
 37. Magyari E, Keller B (1999) Heat and mass transfer in the boundary layers on an exponentially stretching continuous surface. *J Phys D Appl Phys* 32:577. <https://doi.org/10.1088/0022-3727/32/5/012>
 38. Elbashbeshy EMA (2001) Heat transfer over an exponentially stretching continuous surface with suction. *Arch Mech* 53:643–651
 39. Khan SK, Sanjayanand E (2005) Viscoelastic boundary layer flow and heat transfer over an exponential stretching sheet. *Int J Heat Mass Transf* 48:1534–1542
 40. Sajid M, Hayat T (2008) Influence of thermal radiation on the boundary layer flow due to an exponentially stretching sheet. *Int Commun Heat Mass Transf* 35:347–356
 41. Bhattacharyya K (2011) Boundary layer flow and heat transfer over an exponentially shrinking sheet. *Chin Phys Lett* 28. <https://doi.org/10.1088/0256-307x/28/7/074701>
 42. Liu IC, Wang HH, Peng YF (2013) Flow and heat transfer for three-dimensional flow over an exponentially stretching surface. *Chem Eng Commun* 200:253–268
 43. Mustafa M, Mushtaq A, Hayat T, Alsaedi A (2015) Radiation effects in three-dimensional flow over a bi-directional exponentially stretching sheet. *J Taiwan Inst Chem Eng* 47:43–49
 44. Weidman P (2016) Flow induced by exponential stretching and shearing plate motions. *Phys Fluids* 28:113602. <https://doi.org/10.1063/1.4966979>
 45. Ahmad R, Mustafa M, Hayat T, Alsaedi A (2016) Numerical study of MHD nanofluid flow and heat transfer past a bidirectional exponentially stretching sheet. *J Magn Magn Mater* 407:69–74
 46. Patil PM, Latha DN, Roy S, Momoniat E (2017) Double diffusive mixed convection flow from a vertical exponentially stretching surface in presence of the viscous dissipation. *Int J Heat Mass Transf* 112:758–766
 47. Merkin JH, Najib N, Bachok N, Ishak A, Pop I (2017) Stagnation-point flow and heat transfer over an exponentially stretching/shrinking cylinder. *J Taiwan Inst Chem Eng* 74:65–72
 48. Liao S (2004) On the homotopy analysis method for nonlinear problems. *Appl Math Comput* 147:499–513
 49. Liao S (2009) Notes on the homotopy analysis method: some definitions and theorems. *Commun Nonlinear Sci Numer Simul* 14:983–997
 50. Liao SJ (2010) An optimal homotopy analysis approach for strongly nonlinear differential equations. *Commun Nonlinear Sci Numer Simul* 15:2003–2016
 51. Farooq U, Zhao YL, Hayat T, Alsaedi A, Liao SJ (2015) Application of the HAM-based Mathematica package BVP4 on MHD Falkner–Skan flow of nanofluid. *Comput Fluids* 111:69–75
 52. Farooq U, Zhao YL, Hayat T, Alsaedi A, Liao SJ (2015) Series solutions of non-similarity boundary layer flows of nano-fluids over stretching surfaces. *Numer Algorithm* 70:43–59
 53. Farooq U, Zhao YL, Hayat T, Alsaedi A, Liao SJ (2014) Heat and mass transfer of a two-layer flows of third-grade nanofluids in a vertical channel. *Appl Math Comput* 242:528–540
 54. Zhong X, Liao SJ (2017) On the homotopy analysis method for backward/forward-backward stochastic differential equations. *Numer Algorithm* 76:487–519
 55. Hajmohammadi MR (2017) Cylindrical Couette flow and heat transfer properties of nanofluids; single-phase and two-phase analyses. *J Mol Liq* 240:45–55
 56. Hajmohammadi MR (2017) Assessment of a lubricant based nanofluid application in a rotary system. *Energy Convers Manag* 146:78–86
 57. Hajmohammadi MR (2017) Design and analysis of multi-scale annular fins attached to a pin fin. *Int J Refrigeration*. <https://doi.org/10.1016/j.ijrefrig.2017.11.032>
 58. Hajmohammadi MR (2018) Optimal design of tree-shaped inverted fins. *Int J Heat Mass Transf* 116:1352–1360